

# Electrohydrodynamic Enforcement in the Heat and Mass Exchange

Michael A. Reznikov, *Senior Member, IEEE*, Alex Kolessov, Richard Koziol

**Abstract**—The net drag effect of the ionic current in the conductive fluid, electrohydrodynamic (EHD) effect, has been investigated as a space and energy saving technology for the enforced heat and mass management. The electrohydrodynamically enforced evaporation, convection and closed-loop phase-change thermal transfer are analyzed and experimentally evaluated. The emphasis of the investigation was on the maximal efficiency of the consumed power. Significance of EHD phenomena for the energy saving is demonstrated on the examples of temperature stabilization for the solid state lighting and the dewatering of the pulp in the paper industry.

**Index Terms**— Electrostatic devices, Heat pumps, Corona.

## I. INTRODUCTION

**D**UE to the energy barrier for evaporation, the transition from liquid to the vapor phase requires additional enthalpy (latent heat). On the one hand, this allows to extract the heat from the liquid. This phenomenon is widely used in heat pipes and spray cooling because of the isothermal nature of the process. While the phase transition energy is supplied by the cooled material itself, the vapor should be removed to prevent the steady state equilibrium. The vapor removal is supported by the convection that mostly limits the density of mass flow and correspondently the heat flux. The enforced convection usually is achieved by the intensive flow of the carrier gas (for example, the air) that requires useless power consumption because the enormous amount of carrier should be moved together with the vapor. On the other hand, if we need to extract the liquid itself, the additional energy should be applied. Thermal dewatering technologies are much more productive than mechanical or physical property-based techniques but they consume large quantities of energy and require excessive space and capital investment because the elevated temperature is reached in entire dewatered material. Thus the major problem to be solved is the applying of energy directly to vapor while keeping the efficiency of thermally

driven evaporation.

## II. ELECTROSTATIC ENFORCEMENT OF EVAPORATION

### A. Using the Dipole Nature of Vapor Molecule

The asymmetric distribution of electric charges in the vapor molecule (water, alcohols) allows using the dielectrophoresis – the drift of dipoles in the gradient of the electrical field – to directly affect the water vapor by an external electric field. The high gradient of the electrical field can be obtained only near the electrodes with large curvatures but the ionic current through the air stream serves as an additional multipoint distributed absorber because every single ion produces a high field gradient around it. Therefore the enrichment of vapor is created near each micro-electrode [1].

The drift of dipoles with dipole moment,  $\rho_0$ , toward the microelectrode is initiated by the existence of dielectrophoretic force,  $\mathbf{F}_{dph} = \rho_0 \cdot \text{grad} |E|$ , directed to the side of increased field,  $E$ . This force builds the potential energy,  $U$ , of the dipole

$$U(x) = \rho_0 \int_0^{\infty} \text{grad} |E| dx. \quad (1)$$

The stationary distribution of molecules with density,  $n(x)$ , occurs at the equality of drift and diffusion flows:

$$\frac{dn(x)}{dt} = n(x) \frac{\mu}{e} \rho_0 \text{grad} |E| - D \frac{dn}{dx}, \quad (2)$$

where the coefficient of diffusion,  $D = \mu kT/e$ , and  $\mu/e$  is actually the kinematic mobility (average speed at the applied unitary force). From Eq. (1), finally, the classic Maxwell distribution of molecules,  $n = n_{\infty} \exp(U/kT)$ , is obtained.

Assuming a natural dipole moment of the water molecule,  $\rho_0 = 6.6 \cdot 10^{-28} \text{ C} \cdot \text{cm}$  [2], the potential energy of such a molecule at radius,  $R$ , from the point charge,  $q$ , can be calculated by integration of dielectrophoretic force from the distance,  $R$ , to infinity:

$$U_R = \rho_0 \int_R^{\infty} \text{grad} E dr = \frac{\rho_0 q}{\epsilon_0 R^2}. \quad (3)$$

At a given temperature and at the absence of airflow, the pressure of the vapor is proportional to the concentration of vapor molecules, and there is enrichment, induced by field,

$$\gamma = \frac{p_R}{p_V} = \exp\left(\frac{U_R}{kT}\right), \quad (4)$$

Manuscript received April 17, 2009. This work was supported in part by the U.S. Department of Energy under grants DE-FG02-06ER84568 and DE-FG02-08ER85073.

Michael A. Reznikov is with the Physical Optics Corporation, Torrance, CA 90501 USA (phone: 310-320-3088; fax: 310-320-1430; e-mail: mreznikov@poc.com).

Alex Kolessov is with the Physical Optics Corporation, Torrance, CA 90501 USA (e-mail: [akolessov@poc.com](mailto:akolessov@poc.com)).

Richard Koziol is with the Physical Optics Corporation, Torrance, CA 90501 USA (e-mail: [rkoziol@poc.com](mailto:rkoziol@poc.com)).

where indexes R and V are related to the pressure at distance, R, and at an infinite distance in the volume of vapor respectively.

If airflow exists, the Eq. (2) should be included in the Navier-Stokes equation and the enrichment according with Eq. (4) is never achieved because the vapor is constantly moved out. This creates the permanent vapor flow from the evaporation surface and results in the displacement of dynamic equilibrium between evaporation and condensation. As an outcome, the effective evaporation rate (evaporation minus condensation) increases.

### B. Electrohydrodynamic Flow

The airflow can be created by the drag action of ions when the corona discharge occurs in the gas (air) - the impulse and kinetic energy are passed to molecules of the neutral gas due to collisions with drifting ions. In the electrohydrodynamic (EHD) vapor pump, the discharge (corona) current is created from the high curvature, 400 cm<sup>-1</sup>, electrode (tungsten wire) at high voltage. Because the electric field around the electrode wire decreases very sharply with distance, r, as 1/r, gas breakdown occurs only at close proximity to the wire. The discharge current is restricted by the resistance of the non-ionized gas and the density of current decreases with distance as 1/r<sup>2</sup>. Therefore, the ionization is limited to a small area near electrode and outside of the ionization area the current consists of only the single sign charge carriers – positive or negative, which depends on the polarity of voltage that is applied to the corona electrode. In case of the positive corona, electrons are collected by the corona wire, the recombination rate is low and ions mostly reach the other, grounded electrode.

In the inter-electrode gap, the ions collide with neutral molecules, thus passing their kinetic momentum to neutral fluid (gas) molecules. This creates a pumping action that moves the fluid through the system. The force creating an ion driven fluid motion is generated because of the electrostatic force on ions within the inter electrode space. The electrical potential and electrical current in the inter-electrode space of an ion drag pump are described by Poisson's equation for electrostatics:

$$\nabla^2 V = -\rho_E / \varepsilon, \quad (5)$$

and the conservation of charge equation:

$$\nabla \cdot (Kq\vec{E} - D\nabla\rho_E) = 0, \quad (6)$$

where V is electric potential,  $\varepsilon$  is the dielectric permittivity of the medium,  $\rho_E$  is the space charge density, and K is the ion mobility. The electric field is represented by,  $\vec{E} = \nabla V$ .

Once the values for  $\rho_E$  and  $\vec{E}$  are known, the force applied on the ions is also the force per unit volume on the bulk fluid. This is because the collision rate is very large and emitted ions reach a steady state (terminal) velocity in a very short distance, and thus all additional kinetic energy is passed to neutral molecules by collision. Thus, the fluid-accelerating force can be

calculated from:

$$\vec{F}_{ions} = \vec{F}_{body} = \vec{E}q. \quad (7)$$

This bulk body force couples the electrostatic equations to the Navier-Stokes equations that govern the flow of the neutral medium:

$$\nabla \cdot \vec{u} = 0, \quad (8)$$

and:

$$\rho\vec{u} \cdot \nabla\vec{u} = -\nabla P + \mu\nabla^2\vec{u} + \vec{F}_{body}, \quad (9)$$

where P represents the static pressure, and  $\vec{u}$ ,  $\rho$ , and  $\mu$  represent the fluid velocity, density, and viscosity, respectively. Because the transverse Coulomb force on the ions is substantially larger than the longitudinal drag force associated with the bulk fluid motion, all ions (and thus all electrical charge) is collected on the grounded electrode(s) and cannot pass through the system.

### C. Electrostatic Vapor Transporter

The charged mesh vapor pump accelerates the transport of vapors from the evaporation surface. Being used for the evaporative cooling, the vapor pump is in an integral part of the electrostatic thermal transporter because it significantly increases the vapor transport rate from the evaporator in comparison to diffusion-based vapor migration, which is relied upon in conventional heat pipes. The vapor pump employs a charged mesh in between the two terminal surfaces. As the vapors pass through the metallic wire mesh, several molecules collide with field-emitted charge carriers and therefore ionize. The strong electric field developed between the wire mesh and the grounded electrode causes these charged molecules to accelerate away from the evaporation surface. Neutral vapors that pass through the mesh gaps uncharged will also be accelerated when they are bombarded by the charged vapor molecules. The electrostatic vapor transport is further enhanced by dielectrophoretic forces that act on the vapors between the evaporator and the charged mesh. The increased vapor flux out of the evaporating surface will cause a pressure drop that will favor movement of vapors from the evaporation plane, which will increase the rate of vaporization. A mesh electrode is preferable for this application because the molecular density of vapor is low and the extended area coverage mesh ensures maximum vapor flow. Vapors between the evaporator surface and the charged mesh will experience a dielectrophoretic force toward the mesh (prior to becoming electrically charged), which will further increase the vapor transport rate realized by the charged mesh vapor pump.

### D. Electrostatic Atomizer

The evaporation is driven by the difference in pressure of saturated vapor over the liquid phase. This difference can be enhanced because the saturated vapor pressure over the flat,  $p_0$ , and curved,  $p_r$ , surface of the liquid according with Kelvin equation for the drop with curvature, 1/r, and surface tension,

$\gamma: \ln \frac{p_r}{p_0} = \frac{2\gamma V_m}{rRT}$ , where  $V_m$  is the molecular volume and  $R$  is the universal gas constant. As a result, the same vapor pressure in the evaporator (over high curvature surface) is under critical and droplets evaporate but it's also above the critical pressure over the flat liquid surface in the condenser and vapor aggregates into the liquid. This coalescence of small droplets to the bulk liquid is a permanent process because droplets are constantly created by the atomizer.

Small droplets of evaporated liquid can be created electrostatic spray. These charged droplets don't coalesce because of their electrical repulsion. Having a charge also means that these drops can be electrically deflected toward a target.

As it follows from the definition, the ejected fluid should have some electrical conductivity,  $k$ , to be able to accept and distribute the electric charge. The distribution of charge per unit volume, charge density in a fluid,  $\rho_e$ , is described by the conservation equation,

$$\frac{\partial \rho_e}{\partial t} + \nabla \cdot (\mathbf{V} \rho_e) = -\nabla \cdot (k\mathbf{E}), \quad (10)$$

where vectors  $\mathbf{V}$  and  $\mathbf{E}$  are the velocity of the fluid flow and the electric field correspondently. The right side of Eq.(10) presents the density of electric current,  $\mathbf{j} = k\mathbf{E}$ . The electric field is affected by the presence of charge density according with the Laplace's equation

$$\nabla \cdot (\varepsilon_0 \varepsilon \mathbf{E}) = \rho_e + \rho_o. \quad (11)$$

In this expression  $\varepsilon_0$  is the permittivity of free space and  $\varepsilon$  is the dielectric constant (i.e., relative permittivity) and  $\rho_o$  is a charge density coming from other sources such as solid mass particles in a fluid. Free charge density also contributes to the electrical force per unit volume acting on the fluid,

$$\mathbf{F} = \rho_e \mathbf{E} + \frac{1}{2} \varepsilon_0 (\varepsilon - 1) \nabla E^2. \quad (12)$$

The first term in Eq.(12) presents the electrophoresis and arises from the free charge while the second term presents the dielectrophoresis and arises from polarization effects. In a fluid with very small conductivity there is little or no free charge and only the second term can have an influence on the fluid dynamics. On the other hand, if a liquid has sufficient electrical conductivity that free charge accumulates only at its surface, the resulting force is sometimes referred to as electro-capillarity. In the present case of electro-spray we are most interested in semi-conductive liquids in which the conductivity is large enough to allow some free charge to accumulate at liquid surfaces.

Another way to write the force in Eq.(12) is through the Maxwell stress tensor,  $T_{ij}$ ,

$$\begin{aligned} F_i &= \nabla_k T_{ik}, \\ T_{ik} &= \varepsilon E_i E_k - \frac{1}{2} \delta_{ik} \varepsilon E^2 \end{aligned} \quad (13)$$

If free charge accumulates at a free liquid surface it induces a normal component of electric field,  $E_n$ , at the surface. According to the Maxwell stress tensor this results in normal and tangential stresses acting on a liquid surface given by,

$$T_n = \frac{1}{2} \varepsilon_0 E_n^2, \quad T_t = \varepsilon_0 E_n E_t. \quad (14)$$

Typically, the normal stress tends to disrupt a surface if it is large enough to overcome the stabilizing effects of surface tension. From Eq.(14) follows that the tangential stress is important only when there is an significant tangential component of the electric field. Surface tangential stresses induce convective flows and fluid deformations that cannot be generated by distributed body forces.

The right side of Eq.(10) can be converted, using Eq.(11) and ignoring  $\rho_o$ , to a term proportional to the charge density,

$$\frac{\partial \rho_e}{\partial t} + \nabla \cdot (\mathbf{V} \rho_e) = -\frac{k}{\varepsilon_0 \varepsilon} \rho_e. \quad (15)$$

The right hand side implies there is an exponential decay in the charge density at any point in the interior of a conducting liquid, with a characteristic relaxation time of  $\tau = \varepsilon_0 \varepsilon / k$ . Because the permittivity  $\varepsilon_0$  in the numerator of  $\tau$  is very small (e.g.,  $8.854 \cdot 10^{-12}$  F/m in SI units) charge decay is usually very fast, unless the conductivity appearing in the denominator is also very small. Therefore the charge is located on the surface of the liquid in most cases.

The shape of liquid starts to deform from the shape caused by surface tension alone due to the interaction of this charge with the applied electric field,. When the applied voltage is increased and effective Coulomb force approaches a force of the surface tension, a cone shape begins to form with convex sides and a rounded tip. This approaches the shape of a straight cone, which is called a Taylor cone, with a whole angle (width) of  $98.6^\circ$ ,  $2 \cdot \theta_0$ . When a certain threshold voltage has been reached the slightly rounded tip inverts and emits a jet of liquid. The threshold electric field at which emission begins has been characterized by the relationship

$$E_{mit} \approx \sqrt{\frac{2\gamma \cos \theta_0}{\varepsilon_0 r_c}}, \quad (16)$$

where  $\gamma$  is the surface tension of the fluid, and  $r_c$  is the radius of the emitter (needle) orifice. Once airborne, the liquid droplets keep the structural integrity until the surface tension exceeds the electrostatic repulsion of surface charges. Up to a point, known as the Rayleigh limit, surface tension prevents droplet fragmentation. Due to evaporation, however, continuous shrinkage in droplet size increases repulsion proportionally and eventually, the Rayleigh limit is overcome and the droplet undergoes Coulombic explosion, splitting into progeny droplets. The amount of charge,  $q_R$ , at which the Rayleigh limit is exceeded and fission occurs has been described by the mathematical relationship

$$q_R = 8\pi\sqrt{\epsilon_0\gamma r^3}, \quad (17)$$

where r is the radius of droplet.

### III. EXPERIMENT

#### Electrostatic Enforcement of the Paper Drier

The test setup was designed for evaluation of the dielectrophoretic extraction of water during the fabrication of paper. Approximately 3,6004,500 trillion Btu/yr (TBtu/yr), or about 18% of all in-plant energy use in the United States is consumed by thermally driven distillation, evaporation and drying technologies. Due to the enormous demand of industry for dewatering, even 20% decrease of the needed energy will save about 144 TBtu/year (or 4,320 billion USD annually at the current price \$0.60 per therm) at current level of industry production. To the best of our knowledge, this is the first attempt anywhere to apply dielectrophoretic forces to intensify the dewatering of materials.

The setup imitates the industrial steam-drum drier and is equipped with sensors that controlled the temperature, relative humidity, and airflow. The scheme for this setup is shown in Fig. 1 and Fig. 2 presents the photo of device.

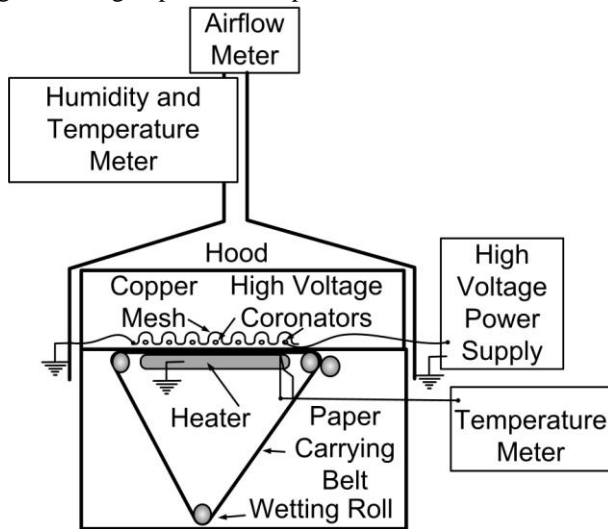


Fig. 1. Test setup for the electrostatic drier enhancer. High voltage coronators serve both as the dielectrophoretic vapor extractors and discharge sources for the electrohydrodynamic pump. Note that the actual electrostatic device is very simple. It consists of the grounded waved mesh and array of thin (50 micrometer) tungsten wires.

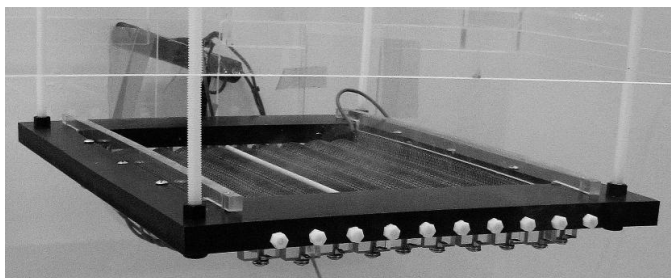


Fig. 2. Electrostatic drier enhancer installed in the acrylic hood for the test of dewatering efficiency.

The test was carried out with the moving belt and permanent constant moistening of the paper. A temperature of the heater (~96°C) was lowered relatively to the used in paper industry to demonstrate the power efficiency of the electrostatic drying. Results of this test are shown in Fig. 3, which clearly demonstrate that the dewatering rate with high voltage applied significantly, about eightfold, exceeds the evaporation due to the heating. Note that we have used the lowered temperature of the heater, ~96°C, instead of the 120°C that is usually used. Therefore, accounting for the 20% temperature decrease, the comparable dewatering improvement should be lowered from 8 times to 6.4 times. But, thermal losses due to the convection also would be lower, due to the decreased temperature difference between the heater and the ambient air. This energy saving can be estimated as  $(96-22)/(120-22) = 75.5\%$  or a 24.5% saving. Moreover, due to the decreased processing time, the total energy saving reaches  $24.5 \cdot 6.4 = 156.8\%$ .

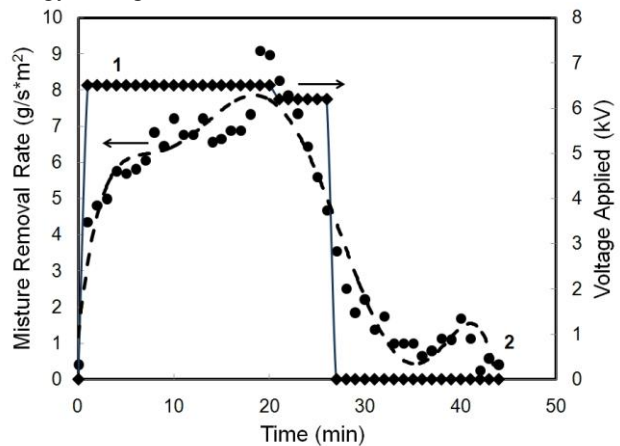


Fig. 3. The dewatering (moisture removal) rate during the dynamic test of electrostatic dryer enhancer.

Of course, we must account for the power consumption of a high voltage power supply that at 6.5 kV output was  $12 \text{ V} \cdot 1.5 \text{ A} = 18 \text{ W}$ . The power consumption of the heater at the stabilized temperature 96°C was ~700 W. Therefore, the final efficiency of the energy saving was  $(700 \cdot 156.8 - 18)/700 = 156.77\%$ , that which is negligibly less than without accounting for the power consumed by the high voltage converter.

#### Electrostatic Enhancement of the Phase-Change Cooling of High Brightness LEDs

While LED's generate little or no infrared (IR) or ultraviolet (UV) radiation and convert up to 25% of the power to visible light, the remainder is converted to heat that must be conducted from the LED die to the underlying circuit board and heat sinks, housings, or luminaire frame elements. As a result, the performance of LED's must rely on heat transfer via conduction or convection, and this insufficient thermal management limits the achievability of benefits from the superior advantages associated with HB LED lighting, such as high energy efficiency, low temperature operation, robustness, digital control, low voltage operation, and long life.

We evaluated the evaporative, phase-change cooling driven by the electrohydrodynamic vapor transport and electrostatic atomization. The technology uses the electrostatic production (Taylor cone effect) of nano-sized droplets of working fluid (alcohol, water) in an electric field to quickly evaporate them on the back side of the LED die, package, or array. Because the latent heat of evaporation is absorbed at constant temperature, the heat removal rate depends only on the circulation of the fluid, which is enforced by electrostatic jet for the liquid phase and electrohydrodynamic (EHD) fans for the vapors. This creates an electrically enforced heat pipe structure. The design of the device is shown in Fig. 4.

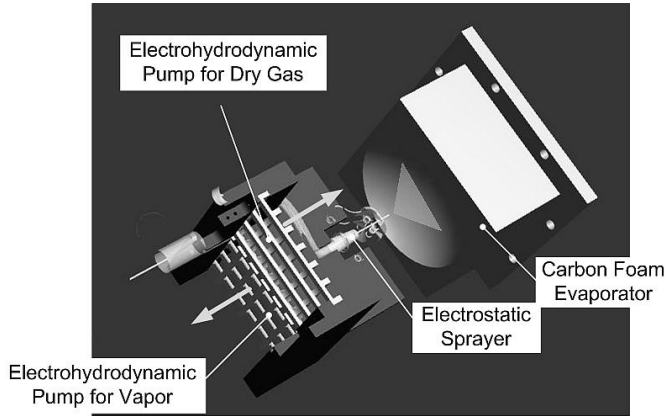


Fig. 4. The design of electrostatic cooler that contains the electrostatic sprayer (atomizer) and electrohydrodynamic driver (pump) for the gas and vapor.

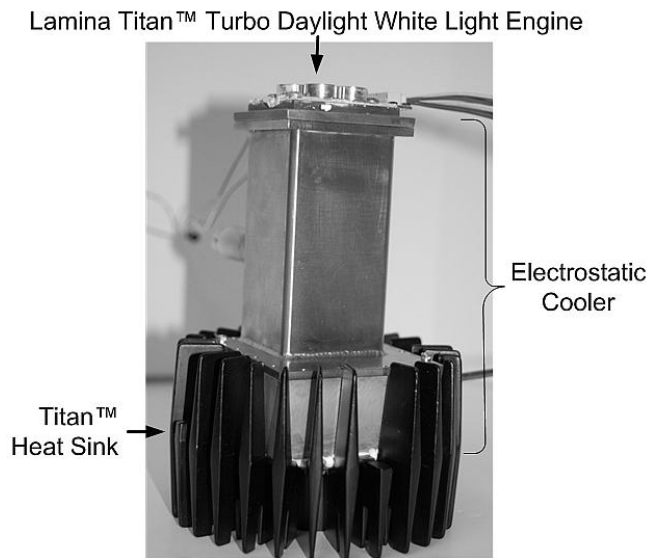


Fig. 5. The electrostatic cooler prototype that cools the LED array by 28°C, which increases the efficacy (light output per consumed power) by 25%.

For the electro spray we tested three working fluids – distilled water, methanol, and ethanol. The volumetric consumption of each fluid at varied voltage applied between the atomizing needle and the evaporator is shown in Fig. 5.

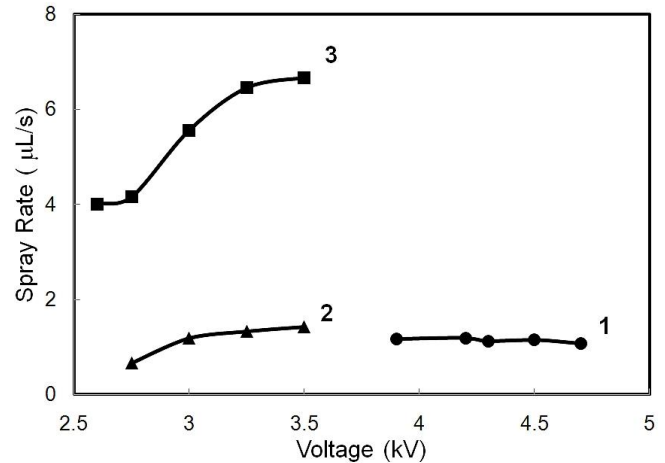


Fig. 5. Spray rate versus applied voltage for the 150-µm needle at distance 36 mm from the concave grounded surface: 1 – distilled water; 2 – ethanol; 3 – methanol.

Fig. 5 shows that the best spraying is achieved with methanol as a working fluid. The saturation of the spray rate with the elevation of applied voltage is clearly observable. This saturation can be explained by the fixed charge surface density at the moment of droplet separation for the given temperature. In this case, the flow rate is limited by the fluid viscosity. Therefore, increasing the voltage leads to the frequent generation of smaller droplets and their higher acceleration, but the total volume of the sprayed fluid does not increase.

The significant difference between methanol and ethanol, despite a practically similar surface tension and density and only a 30% difference in the latent heat of evaporation, is created by the huge difference in the spraying rate, 4.86 times. We attribute this to the higher positive charge affinity (lower barrier for the extraction of an electron) of methanol than that of ethanol. Despite the high latent heat of evaporation, water is sprayed too poorly and at too high a voltage, which results in a low cooling rate. It should be noted that this test was carried out at room temperature (22°C), and using water at significantly higher temperatures is not excluded due to the lowering of surface tension.

Because the spraying rate at the simplified, bi-electrode configuration is too sensitive to position a second, collecting electrode (evaporator in our case), we tested the atomizer with an additional, extracting electrode that is a ring installed in front of the needle tip. Four configurations of the electrostatic sprayer were tested where the extracting ring electrode (diameter 6 mm) was placed at a fixed distance from the collector (20 mm), while the distance from the needle tip to the ring was varied – 2 mm, 4 mm, 6 mm, and 10 mm. Fig. 6 shows results of this test with the methanol.

This test revealed that the practically transversal extracting field (at 2-mm distance) is notably more effective than the additional longitudinal field (at 100-mm distance). This additional field affects the separation of the drops in two ways – decreasing the surface tension at the needle tip (negative electrowetting effect) and applying additional force toward the

evaporator. The first effect prevails at short distances to the ring (2 mm) but the second effect works when the distance to the ring is comparable to the diameter of this ring (6 mm). The effect at the intermediate distance (4 mm), or at too long distance (10 mm), is notably lower.

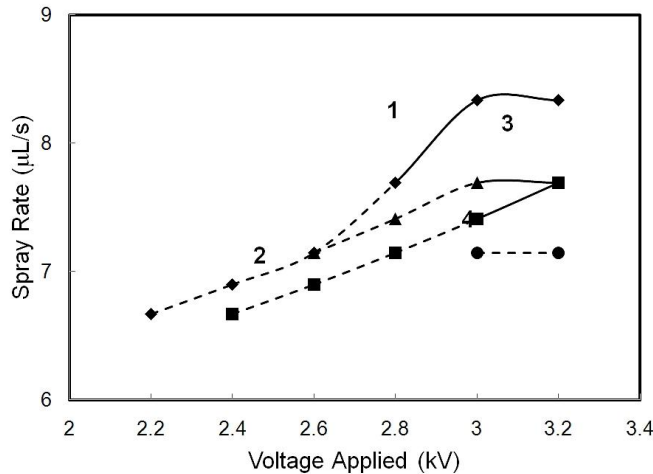


Fig. 6. Spray rate versus applied voltage for methanol at varied distance to the extracting electrode: 1 – 2 mm, 2 – 4 mm, 3 – 6 mm, and 4 – 10 mm. The dotted line shows the dripping regime.

The extracting electrode practically does not collect the spray charge because fluid is ballistically pulled through the ring. Nevertheless, each charged droplet induces a charge of opposite sign in this electrode when it passes the ring. Fig. 7 shows typical signals produced by charged drops in the extracting and collecting electrodes.

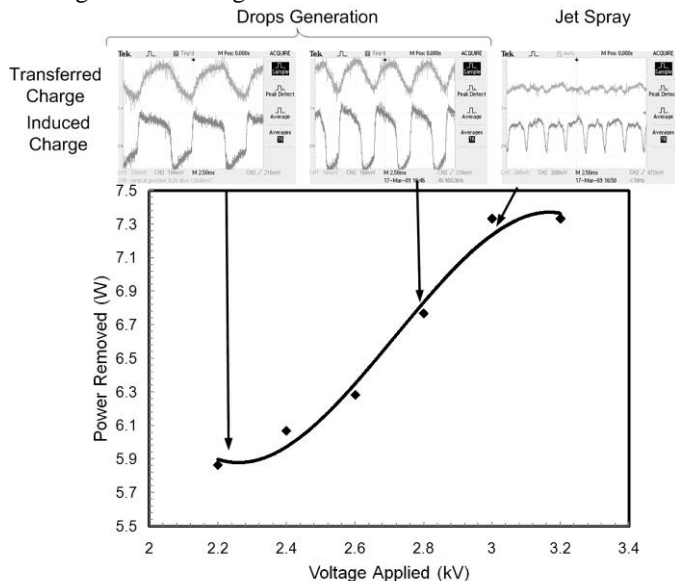


Fig. 7. Total removed power by the electrostatic atomizing of methanol at varied applied voltage with illustration of signals from the transferred and induced charge. The first 2 oscillograms show the clear dripping (emission of single drops) while last oscillogram demonstrate the jet spray regime.

It is notable that pulses in Fig. 7 are synchronized, which means that corresponding pairs of pulses are produced by the same droplet. The pulse of a transferred charge reflects the discharge of the droplet that produces the pulse of the single polarity.

In contrast to this, the induced pulse is bipolar, which reflects the induction of charge (positive current) when the droplet moves toward the plane of the electrode and the relaxation of charge (negative current) when the droplet moves away from the electrode. This technique allows monitoring the frequency of drops generation and estimates the average charge per droplet. Therefore, the transition from the dripping regime (generation of a relatively big droplet) to the spray regime (disintegration of the Taylor cone to the plume of nano-droplets) can be monitored in this simple way. Please note in Fig. 7 that induced charge pulses are always bipolar while the transferred charge exposes the significant constant bias component in the jet spray regime when signals of nano-droplets in the charged plume are indistinguishable.

#### IV. CONCLUSION

Electrostatic evaporation systems have the number of advantages over the current dewatering technologies due to the saving of consumed power, compactness, reduced cost and environmentally friendliness. This technique converts challenging water properties to the useful driving forces. For example, the polarity of water molecules increases the heat of evaporation in the thermal technology but this polarity allows moving of water vapor toward microelectrodes in the electrostatic evaporation system.

Unlike current cooling systems that provide heat energy flow solely due to the temperature gradient, the electrostatic system increases the chemical potential of the heat-carrier fluid by introducing a high surface-to-volume ratio and high curvature of surface in nano-sized droplets. The resulting gradient of vapor chemical potential between the heat extracting evaporator and heat releasing condenser efficiently supports a high rate of phase conversion. Thus, the heat extraction process (evaporation) is isothermally driven by the extracted thermal energy itself. The matching mass transport is achieved by the utilization of ions scattering on molecules of vapor and carrier gas (air or helium). This not only highly intensifies thermal exchange but also creates the possibility to minimize the temperature of the cooled hot spot, even to the ambient temperature, because the driving force for the heat extraction is the phase change process. Thus, this technology can be considered as a reversible, permanently self-regenerating coalescence technology that provides improved efficacy due to the isothermal heat management of the power dissipating device while consuming minimal power for the mass transport because electrostatic forces are applied directly to the working fluid.

#### REFERENCES

- [1] M. Reznikov, "Dielectrophoretic Dehumidification of Gas Stream in Low and Moderate Electrical Fields," Presented at ESA-IEEE Joint Meeting of Electrostatics, Little Rock, AR, June 24-27, 2003, pp. 230-240.
- [2] G. Maroulis, "Hyperpolarizability of H<sub>2</sub>O," *J. Chem. Phys.*, vol. 94, 1991, pp. 1182-1190.